

KSP 2021

SIMULATION OF ASTEROID BELT AND KIRKWOOD GAPS

August 29, 2021

Sahil Saha

Amrit Putcha

Contents

1	Introduction	3
2	Theoretical Background	3
2.1	Three Body Problem	3
2.2	N-Body Problem	3
2.3	Restricted Three Body Problem	3
3	Calculation of Trajectory of an Asteroid	4
4	Potential Plot in Restricted Three Body Problem	5
5	Analysis of Lagrange Points	6
5.1	Location of Lagrange Points	6
5.2	Stability of Lagrange Points	7
6	Method of Integration	7
7	Trajectories for a Single Body	9
7.1	Placement in L4	9
7.2	Horseshoe Orbit	10
7.3	Placement at other points	10
8	Initial Distribution of Asteroids	11
9	Trojan, Greek and Hilda Groups	12
10	Formation of Asteroid Belt and Gaps	13
11	Simulation of the Asteroid Belt	13
11.1	Simulation for 10,000 years	14
11.2	Simulation for 100,000 years	15
11.3	Simulation for 380,000 years	16
11.4	Figures for Other Time Intervals and Histograms for Average distance from the Sun	17
12	Discussion on why Gaps are not Visible in the Main Belt Simulations	18
13	Scope for More Precise Results and Further Applications	19
14	Conclusion	20
15	Repository for Code Used for Simulation	20

1 Introduction

The report involves a detailed study of the formation of the Asteroid Belt in between Jupiter and Sun considering the gravitational effects and studying the formation of zones of relatively low asteroid concentration, deemed as *Gaps*. In course of simulating the said systems in Fortran, we have encountered the Restricted Three Body Problem as the primary tool to trace the trajectories of a small mass (negligible compared to the solar mass and planets) and using a random sampling, we have generated initial conditions of 120,000 such small bodies and extracted results for different time periods.

2 Theoretical Background

2.1 Three Body Problem

The widely studied Three Body Problem begins with the necessity of analysing three independent masses with certain initial conditions attached to them. Under the gravitational effects of three bodies, the positions and velocities rapidly change resulting in chaotic trajectories. An analytical approach towards this problem fails owing to the number of variables involved in the calculations and most commonly, methods of numerical computation like Euler Method and Runge Kutta Order-4 are used to trace out the trajectories. As we are dealing with conservative forces, all the said integrators give satisfactory results. However, due to the chaotic nature, extreme precision and repetitive computation is needed to consider perfect trajectories.

2.2 N-Body Problem

Simulating an Asteroid Belt with hundreds of thousands of individual masses requires an approach towards the N-Body problem involving N masses interacting with each other. Analytically, this proves to be impossible to solve completely and thus once again numerical integration is widely used. However, the computational power required when performing this is beyond what can be handled by privately owned computers.

2.3 Restricted Three Body Problem

Even though the problem of three interacting masses cannot be ideally solved, we can simplify the problem down to something analytically solvable when considering the Sun, Jupiter and a single asteroid. The assumptions are that :

- Jupiter is travelling in a circular orbit around the sun with angular frequency ω .
- The mass of the asteroid is negligible compared to the other two bodies and thus its gravitational effects too can be ignored.
- The entire frame of reference in which the calculations are performed is considered to be rotating with angular frequency ω , resulting in a frame where the Sun and Jupiter can be considered to be still

3 Calculation of Trajectory of an Asteroid

In a frame of reference rotating with angular frequency ω we fix a mass M_1 at the origin around which M_2 rotates in circular motion with the same angular frequency, thus effectively being at rest [1].

The origin is considered to be the Centre of Mass of these two masses, thus we can place M_1 at $(-\frac{M_2 R}{M_1 + M_2}, 0)$ and M_2 at $(\frac{M_1 R}{M_1 + M_2}, 0)$. The masses are R units apart.

We consider the negligible mass m to be at (x, y) at any point of time.

Let,

$$r_1 = \frac{M_2 R}{M_1 + M_2}, r_2 = \frac{M_1 R}{M_1 + M_2}$$

The Lagrangian for m when it is at (x, y) for an inertial frame is given by:

$$L = T - V = \frac{1}{2}m(\dot{x}^2 + \dot{y}^2) + \frac{GmM_1}{((x + r_1)^2 + y^2)^{\frac{1}{2}}} + \frac{GmM_2}{((x - r_2)^2 + y^2)^{\frac{1}{2}}}$$

Now to consider the rotating frame, we must take x' and y' such that:

$$x' = x\cos(\omega t) - y\sin(\omega t)$$

$$y' = x\sin(\omega t) + y\cos(\omega t)$$

Changing x' and y' to x and y respectively, we obtain the final equations:

$$L = T - V = \frac{1}{2}m(\dot{x}^2 + \dot{y}^2 + 2\omega x\dot{y} - 2\omega y\dot{x} + \omega^2(x^2 + y^2)) + \frac{GmM_1}{((x + r_1)^2 + y^2)^{\frac{1}{2}}} + \frac{GmM_2}{((x - r_2)^2 + y^2)^{\frac{1}{2}}}$$

Viewing the terms individually, we get the potential in this frame

$$V = -\frac{1}{2}m\omega^2(x^2 + y^2) - \frac{GmM_1}{((x + r_1)^2 + y^2)^{\frac{1}{2}}} - \frac{GmM_2}{((x - r_2)^2 + y^2)^{\frac{1}{2}}}$$

Using the equation below for x and y :

$$\frac{d}{dt}\left(\frac{\partial L}{\partial \dot{u}}\right) = \frac{\partial L}{\partial u}$$

We get :

$$\begin{aligned} \ddot{x} &= 2\omega\dot{y} + \omega^2x - \frac{GM_1(x + r_1)}{((x + r_1)^2 + y^2)^{\frac{3}{2}}} - \frac{GM_2(x - r_2)}{((x - r_2)^2 + y^2)^{\frac{3}{2}}} \\ \ddot{y} &= -2\omega\dot{x} + \omega^2y - \frac{GM_1y}{((x + r_1)^2 + y^2)^{\frac{3}{2}}} - \frac{GM_2y}{((x - r_2)^2 + y^2)^{\frac{3}{2}}} \end{aligned}$$

Substituting the masses of Sun and Jupiter for M_1 and M_2 we can obtain the trajectory for an asteroid under their effect in this rotating frame of reference.

4 Potential Plot in Restricted Three Body Problem

From the derived Lagrangian for the two bodies, we have obtained the velocity independent terms and their sum is mathematically the potential due to the Sun and Jupiter for adjusted parameters. In order to obtain the angular frequency we use the initial distance from Sun to Jupiter as R and we can obtain $\omega = \sqrt{\frac{GM_{sun}}{R}}$, thus $\omega = 1.68 \times 10^{-8} rad/s$.

However, due to the difference in mass of the Sun and the planet, we cannot correctly view the potential difference across the points and have displayed a considerably scaled down system where two masses are 1 and 10 units, the distance between them is 1 unit, $G = 1$ and ω is calculated using the previously mentioned expression. The centre of mass and distances of corresponding bodies are adjusted accordingly and the final potential is scaled down by 10. All values considered for the final plot are absolute values and the negative sign is not considered in the figure.

From the equation derived in Section 3 we have the equation and the corresponding plot

$$V = -\frac{1}{2}m\omega^2(x^2 + y^2) - \frac{GmM_1}{((x + r_1)^2 + y^2)^{\frac{1}{2}}} - \frac{GmM_2}{((x - r_2)^2 + y^2)^{\frac{1}{2}}}$$

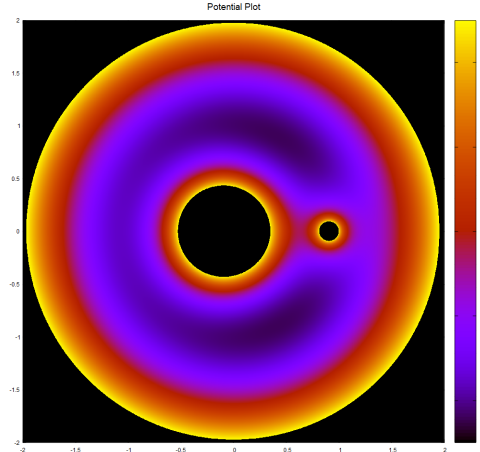


Figure 1: The above figure gives us the potential plot for the restricted 3 body problem. The reference frame taken is a rotating frame where the two heavy masses are considered to be fixed and the origin is at the center of mass of the two bodies.

The area of the plot which has been blackened includes potential which is higher than a threshold (here 0.25) thus allowing us to view the resulting observable difference in different regions.

There are various points to be noted over the plot, the two most important being the darker spots above and below the relatively smaller mass and three points, one to the left of the larger mass, one between the two and the third to the right of the smaller mass. All

these points are characterised by the fact that in those points there exists a local extremum, ie, $\nabla V = 0$ indicating that forces are completely balanced in those 5 points and the question of stability near the 5 points arises. These points are called Lagrange Points.

5 Analysis of Lagrange Points

The method of solving also gives rise to a few special points that remain stationary with respect to the frame of reference i.e. all the forces acting cancel out giving rise to zero relative motion.

Such special points are known as Lagrange points. There are mathematically 5 such points existing in the plane of orbit of the two heavier objects, and these are labelled from L1 to L5 respectively. Two of these are stable (L4, L5) and three of which are unstable (L1, L2 and L3).

A representation of the Lagrange points of the earth-sun system is shown in the figure below

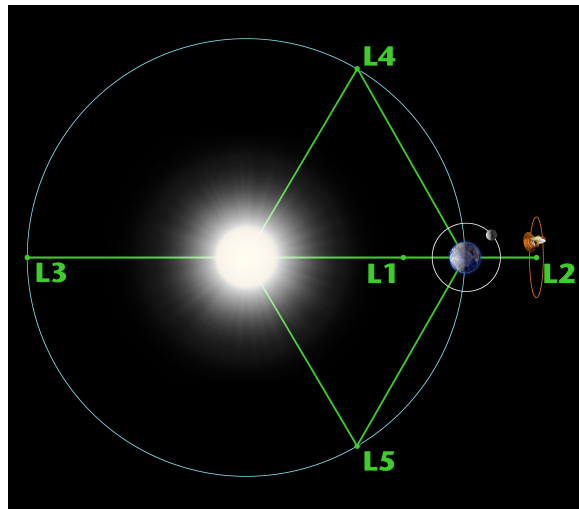


Figure 2: Lagrange points labelled L1 to L5 for the earth-sun system. (Source : NASA)

5.1 Location of Lagrange Points

We can define the plane they move in, to be the x-y plane with both heavier masses on the x-axis and with the origin at the center of mass. Let R be the distance between m₁ and m₂, we then have the positions of the two heavier masses as:

$$r_1 = \left(\frac{-M_2 R}{M_1 + M_2}, 0, 0 \right), r_2 = \left(\frac{M_1 R}{M_1 + M_2}, 0, 0 \right)$$

Calculating the coordinates, one obtains:

$$L1 = \left(R \left(1 - \left(\frac{\alpha}{3} \right)^{1/3} \right), 0 \right)$$

$$L2 = \left(R \left(1 + \left(\frac{\alpha}{3} \right)^{1/3} \right), 0 \right)$$

$$\begin{aligned}
L3 &= \left(-R\left(1 - \left(\frac{5\alpha}{12}\right)^{1/3}\right), 0\right) \\
L4 &= \left(\left(\frac{R}{2}\right)\left(\frac{m_1 - m_2}{m_1 + m_2}\right), \frac{\sqrt{3}}{2}R, 0\right) \\
L5 &= \left(\left(\frac{R}{2}\right)\left(\frac{m_1 - m_2}{m_1 + m_2}\right), -\frac{\sqrt{3}}{2}R, 0\right)
\end{aligned}$$

where $\alpha = \frac{M_2}{M_1 + M_2}$

5.2 Stability of Lagrange Points

In contrast to L4 and L5, where stable equilibrium exists, the points L1, L2, and L3 are positions of unstable equilibrium. Any object orbiting at L1, L2, or L3 will tend to fall out of orbit; it is therefore rare to find natural objects there, and spacecraft inhabiting these areas must employ station keeping in order to maintain their position.

The L4 and L5 points lie at the third corners of the two equilateral triangles in the plane of orbit whose common base is the line between the centers of the two masses, such that the point lies behind (L5) or ahead (L4) of the smaller mass with regard to its orbit around the larger mass.

6 Method of Integration

In order to calculate the trajectory following the derived equations in the restricted three body problem, we need to find a suitable algorithm. The methods commonly used include Runge-Kutta Fourth Order Method and Euler Method. However, we also attempted symplectic methods including Velocity Verlet Algorithm and Symplectic Euler Method. However, there are issues with all of these commonly used methods, especially concerning symplectic methods.

For the Euler Algorithm, it was not used as its accuracy is acceptable only over small time steps and a small time of calculation. We needed to simulate for 10,000 to 100,000 years for acceptable results and considered a 7-14 day time step which was not compatible.

For symplectic methods, the primary requirement is that the Hamiltonian of the system is preserved. In our case, the Hamiltonian has the expression :

$$H = T + V = \frac{1}{2}m(\dot{x}^2 + \dot{y}^2 + 2\omega x\dot{y} - 2\omega y\dot{x}) - \frac{1}{2}m\omega^2(x^2 + y^2) - \frac{GmM_1}{((x + r_1)^2 + y^2)^{\frac{1}{2}}} - \frac{GmM_2}{((x - r_2)^2 + y^2)^{\frac{1}{2}}}$$

From this, we notice that the acceleration obtained is velocity dependent, of the form :

$$\begin{aligned}
\ddot{x} &= 2\dot{y} + x - \frac{\mu(x + \mu')}{((x + \mu')^2 + y^2)^{\frac{3}{2}}} - \frac{\mu'(x - \mu)}{((x - \mu)^2 + y^2)^{\frac{3}{2}}} \\
\ddot{y} &= -2\dot{x} + y - \frac{\mu y}{((x + \mu')^2 + y^2)^{\frac{3}{2}}} - \frac{\mu' y}{((x - \mu)^2 + y^2)^{\frac{3}{2}}}
\end{aligned}$$

Thus, the Hamiltonian is not conserved and the actual conserved quantity in our case turns out to be [2] :

$$c = (\dot{x}^2 + \dot{y}^2 - x^2 - y^2) - \frac{\mu}{((x + \mu')^2 + y^2)} - \frac{\mu}{((x + \mu')^2 + y^2)}$$

And upon calculation we can see that the magnitude of energy rapidly increases with general symplectic methods thus rendering them unusable for any large span of time.

Coming to the implementation of Runge Kutta 4th order methods, we can see a high stability of the energy over a long span of time in the problem, providing accurate results, however in the range of 10,000 and above years with a 14 day time step, there is a small upward trend in the energy magnitude, thus it was not used.

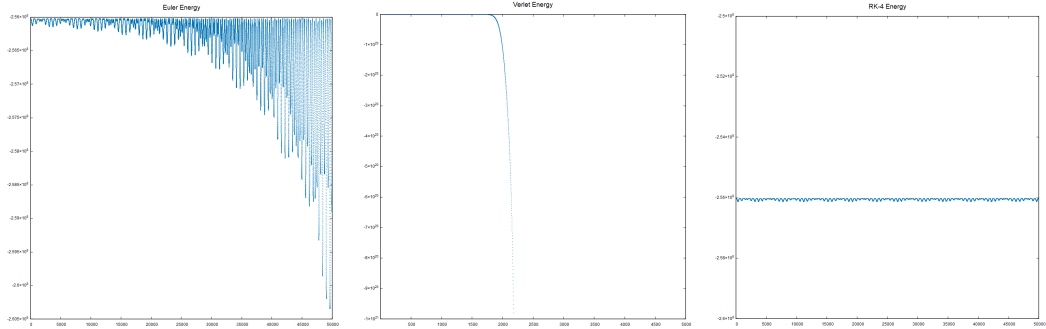


Figure 3: The above set of figures give us the comparison between three integrators, namely the Euler, the Verlet and the RK4 integrator. Even though RK4 looks very accurate, there are specific problems with RK4 which is explained in the paragraph above.

The final method of integration is a modification of the Euler method to include a midpoint, giving rise to the Euler-Richardson Algorithm. For the acceleration function $a = a(x, \dot{x})$, the method looks as follows:

$$\begin{aligned} a_n &= a(x_n, \dot{x}_n) \\ \dot{x}_{mid} &= \dot{x}_n + \frac{1}{2}a_n\Delta t \\ x_{mid} &= x_n + \frac{1}{2}\dot{x}_n\Delta t \\ a_{mid} &= a(x_{mid}, \dot{x}_{mid}) \end{aligned}$$

For the final value of the position and velocity :

$$\begin{aligned} \dot{x}_{n+1} &= \dot{x}_n + a_{mid}\Delta t \\ x_{n+1} &= x_n + v_{mid}\Delta t \end{aligned}$$

For our calculations, this method of computing gave the most accurate results with deviation of maximum and minimum relative to the average being $\frac{\delta E}{E} = 4.14 \times 10^{-4}$.

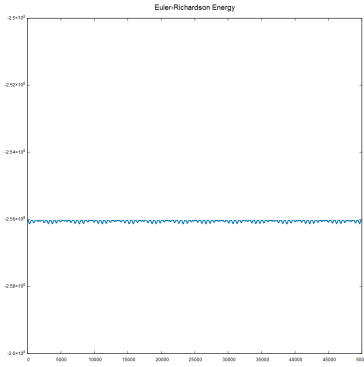


Figure 4: The above plot shows the deviations energy caused when we use the Euler-Richardson Algorithm are very small and this algorithm works best for our simulation.

7 Trajectories for a Single Body

7.1 Placement in L4

We first consider the case of an asteroid placed exactly on L4 of the Sun-Jupiter system. From the mathematical analysis of Lagrange points, it should be the case that the body is restricted near L4 itself. We first observe the quasi periodic oscillation of the body around L4.

The mass of the Sun and Jupiter are 1.989×10^{30} kg and 1.898×10^{27} kg respectively. The two bodies are at a separation of $5.2AU = 7.8 \times 10^{11}m$. The angular velocity of the rotating frame is $\omega = 1.672 \times 10^{-8}rad/s$. The simulation is performed at a time step of 7 days for nearly 10,000 years.

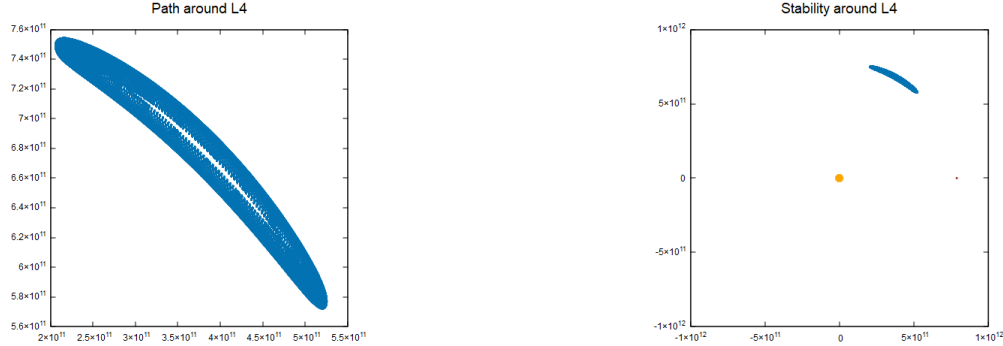


Figure 5: For the figure on the right, the stability was considered for 100,000 years and we see a perfect restriction around L4 for the same time gap of calculation.

For the stable L5 point, we will obtain similar results on the negative Y-axis of the plot.

7.2 Horseshoe Orbit

We can find a particular orbit of interest if we inspect another asteroid position where we place the small mass just slightly away from the L4 or L5 points.

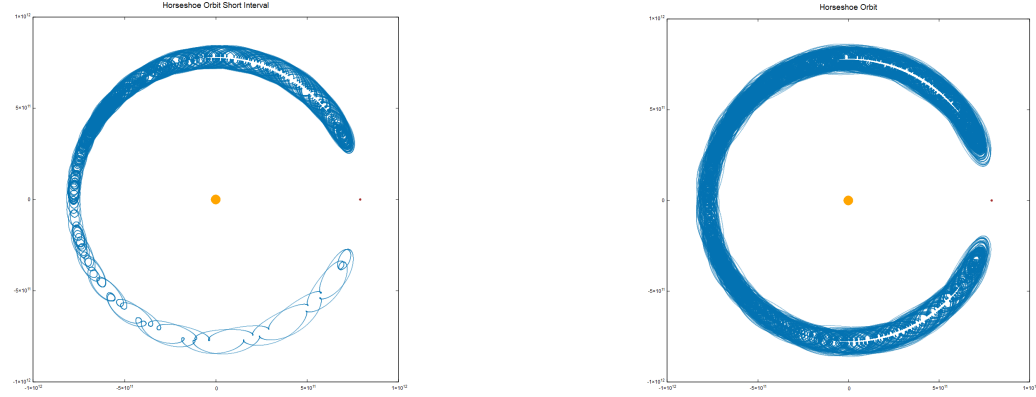


Figure 6 : The left figure shows the initial phases of Horseshoe Orbit formation originating from L4 and the right figure displays the trajectory between L4,L3 and L5 for a longer span.

Here we present two figures where the initial position of the smaller body is 1.015 times the x-coordinate and 1.006 times the y-coordinate of L4. From the left figure which is done for a time span of about 9,600 years we notice that the body starts a similar quasi-periodic orbit around L4 like in the previous case, but soon, it gains a velocity sufficient to exit the low potential region and follows a spiralling motion away towards L3 and exceeds the unstable L3 point to be captured by L5. After reaching L5, it is drawn back again and retraces the path in the opposite direction.

From the other figure which accounts for 40,000 years, we see that the body travels to and from L4, L5 crossing L3 in a *Horseshoe* shaped orbit, being confined there.

7.3 Placement at other points

Below we provide four plots for a third body placed near L1, L2 and L3. We can see that for all the cases, there is some restricted orbit for a short period of time but once the object gets close to either the Sun or Jupiter, it does not return. The placement on L3 results in another Horseshoe orbit like near L4 but without a spiral motion induced by the stable Lagrange points.

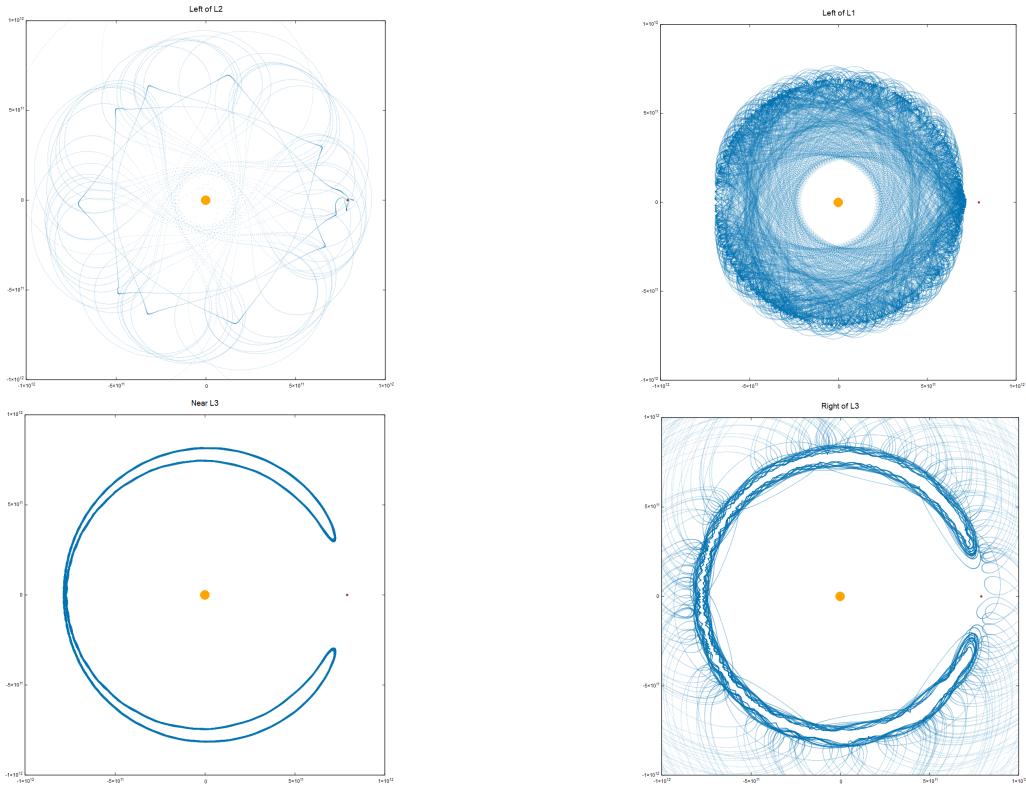


Figure 7: From Top Left, the trajectory for placement to the left of L2, Top Right, origin to the left of L1, Bottom Left, Horseshoe Orbit from near L3 and Bottom Right, unbounded trajectory with origin near L3.

8 Initial Distribution of Asteroids

The main asteroid belt is placed in between Sun and Jupiter. In order to account for this in the simulation, 120,000 asteroids were considered to be uniformly distributed in radial range of 1×10^{11} to 10×10^{11} in all directions.

The rotation in circular orbits around sun was considered for each of them and initial velocities were provided according to the following equations:

$$\dot{x}_i = -y_i \left(\sqrt{\frac{GM_s}{x(i)^3}} - \omega \right), \dot{y}_i = x_i \left(\sqrt{\frac{GM_s}{x(i)^3}} - \omega \right)$$

We show the plot of the initial distribution below:

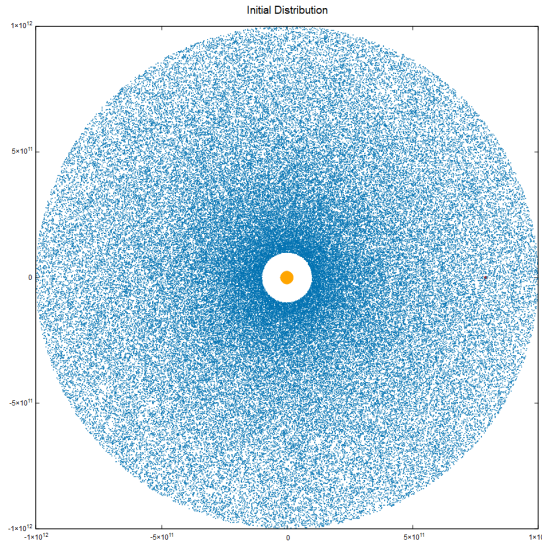


Figure 8: Initial Distribution of Asteroids

9 Trojan, Greek and Hilda Groups

An accumulation of asteroids near the L4 is called the 'Greek' group and near L5 it is termed as 'Trojan' Group. These asteroids accumulate due to the stability of the Lagrange points and are accompanied by the 'Hilda' asteroid group which shows a roughly triangular formation with the individual bodies travelling from L4 to L3 to L5 and back to L4 in a cyclic manner. These asteroids are in 3:2 orbital resonance with Jupiter, that is they orbit 3 times for 2 times of one Jupiter Orbit.

We can see these groups individually by setting initial velocities of all asteroids to zero and using our Fortran code for 100,000 years in a 14 day time step.

Locations of the involved Lagrange Points :

L4 : (3.89e11, 6.754e11)

L5 : (3.89e11, -6.754e11)

L3 : (-7.8234e11, 0)

Other than the predicted Trojan and Greek accumulation near L4 and L5, there is also a smaller accumulation of simulated asteroids near L3. The probable reasons for this is the fact that it is a transition point for the travelling Hilda group and also the fact that any observed Horseshoe orbits narrow down near L3 again owing to it being a transition point.

The simulated plot of the three asteroid groups is given below where all 3 separate groups are visible.

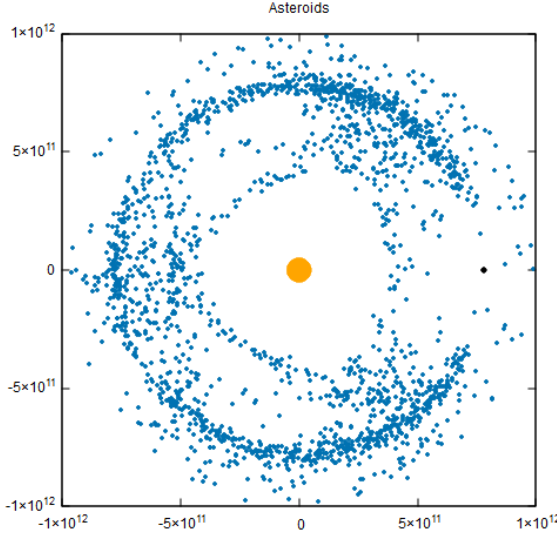


Figure 9: Trojan, Greek and Hilda Asteroid Groups

In course of the simulation we lose nearly 90% of our initial asteroids and also cannot observe the formation of an actual belt owing to the fact that we have not considered initial circular orbits for any of the bodies and thus they come too close to either Jupiter or the Sun, and are ejected at high velocities.

10 Formation of Asteroid Belt and Gaps

Kirkwood gaps, interruptions that appear in the distribution of asteroid semi-major axes where the orbital period of any small body present would be a simple fraction of that of Jupiter. Several zones of low density in the minor-planet population were noticed about 1860 by Daniel Kirkwood, an American mathematician and astronomer, who explained the gaps as resulting from perturbations by Jupiter. An object that revolved around the Sun in one of the gaps would be disturbed regularly by Jupiter's gravitational pull and eventually moved to another orbit. Some of those gaps are the primary sources of the near-Earth asteroids, which form from collisions between main-belt asteroids located close to a Kirkwood gap.

11 Simulation of the Asteroid Belt

The parameters used for the final simulation are listed below :

- Mass of Sun : 1.989e30 kg
- Mass of Jupiter : 1.898e27 kg
- Angular Velocity of Rotating Frame : 1.672e-8 rad/s
- Gravitational Constant : 6.67e-11 unit
- Position of Sun : (-743604142,0)

- Position of Jupiter : (7.7926e11,0)

The initial conditions were set according to the values in the uniform distribution mentioned in Section 8 and similarly selected values of velocity.

We analyse the final results for different time gaps to obtain a better idea regarding the formation of the actual asteroid belt and gaps.

11.1 Simulation for 10,000 years

We first run our simulation at a 7 day time step for 520,000 counts thus obtaining around 10,000 years change of positions.

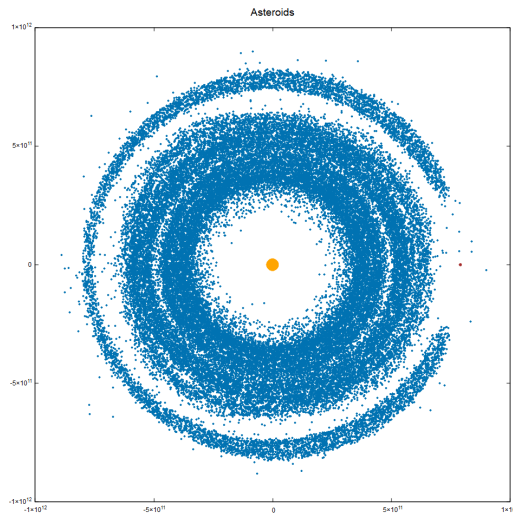


Figure 10.1 : Final Position of Asteroids after 10,000 years

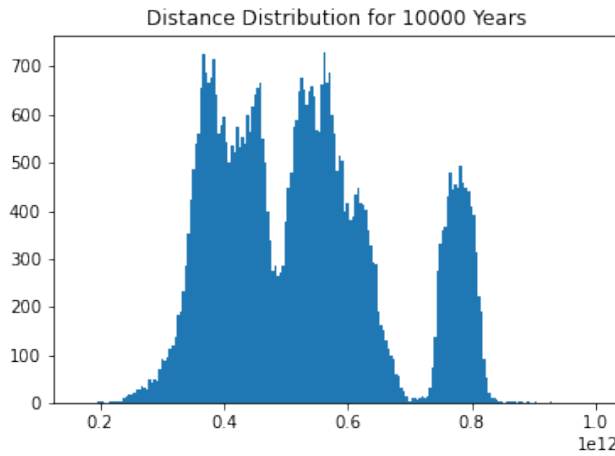


Figure 10.2 : Number of Asteroids against Distance from the Sun

From the figure we can see that as expected there is an accumulation of a large number of asteroids near L4 and L5 lagrange points with a few transitioning along L3. There is a formation of a clear inner belt with varying number of concentration of simulated points

and an especially low concentration around the 4.75×10^{11} m distance. There are secondary dips around 3.75×10^{11} to 4×10^{11} and around 6×10^{11} metres too. The prominent gap in the neighbourhood of 7×10^{11} metres is the separation of the inner belt and the outer asteroids along the Jupiter orbit.

11.2 Simulation for 100,000 years

Now we move ahead to 100,000 years where stabilisation of the asteroid orbit starts. We obtain the following figures for a 7 day timestep and 5,200,000 counts thus going to nearly 100,000 years.

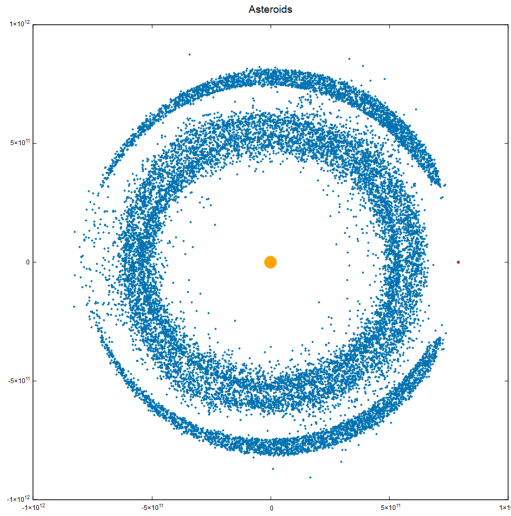


Figure 11.1 : Final Position of Asteroids after 100,000 years

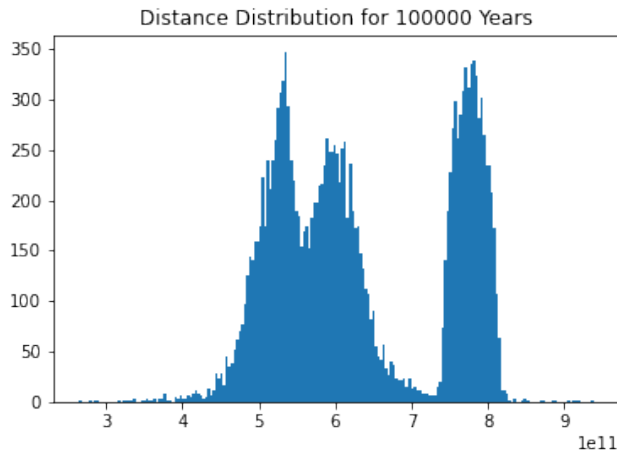


Figure 11.2 : Number of Asteroids against Distance from the Sun

Here we can also observe similar results with a prominent gap past 7×10^{11} m where the demarcation between the inner and outer belt is observed by extremely low number of asteroids. Near towards 5.5×10^{11} m we observe the previously seen minima of number of asteroids and two consequent peaks on either side. The main belt seems to start at around 5×10^{11} m and extends to 7×10^{11} m.

11.3 Simulation for 380,000 years

Approaching 380,000 years we can see that the asteroids are in stable orbits and follow an expected pattern. The time step is again 7 days and the count has been adjusted accordingly.

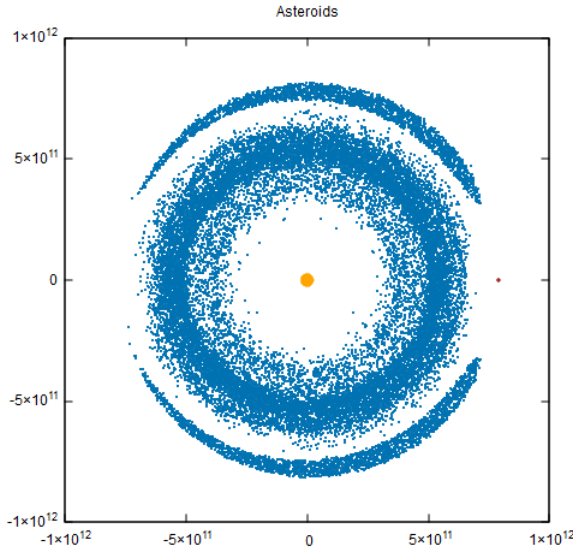


Figure 12.1 : Final Position of Asteroids after 100,000 years

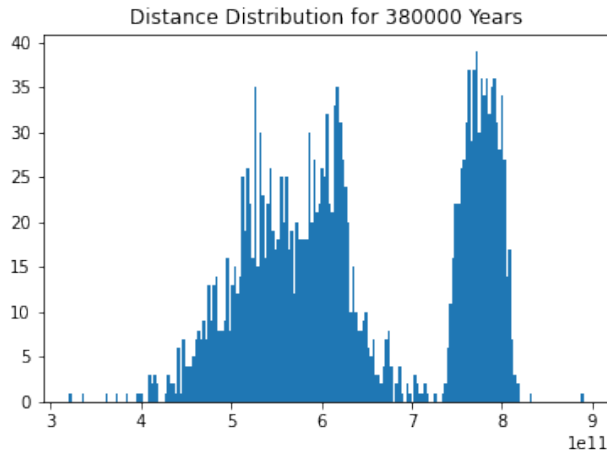
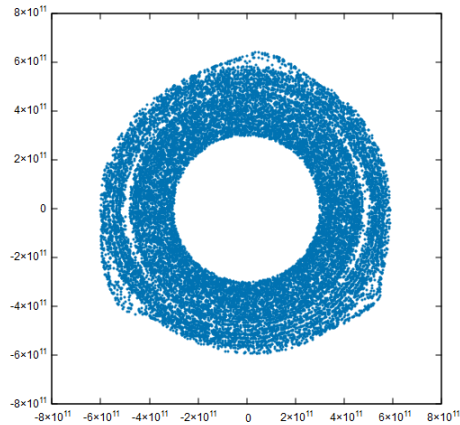


Figure 12.2 : Number of Asteroids against Distance from the Sun

However, we see no distinct minima in this case but there are periodic dips which follow the trend of the previous two figures. The main belt extends from 4×10^{11} m to 7×10^{11} m with the primary minima being near 5.5×10^{11} .

11.4 Figures for Other Time Intervals and Histograms for Average distance from the Sun

The simulated images found other than described ones are given below :



**Figure 13.1 : Final Position of Asteroids after 15,000 years
Outer Asteroids not included**

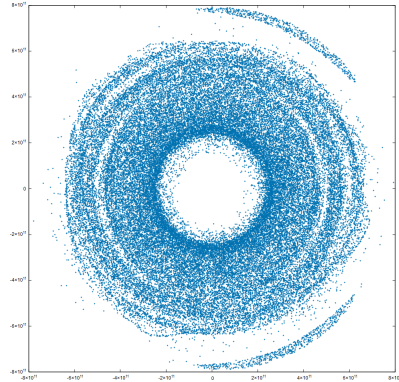
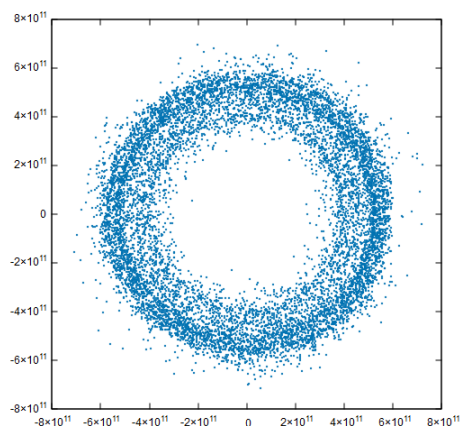


Figure 13.2 : Final Position of Asteroids after 5000 years



**Figure 13.3 : Final Position of Asteroids after 15,000 years
Outer Asteroids not included**

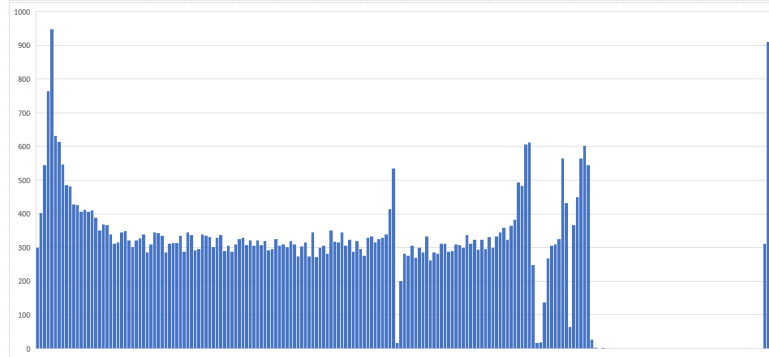


Figure 13.4 : Average Distance from sun for Asteroids over 5,000 years
The X-axis ranges from 0 to $1e12$ metres from the Sun.
Initial Gaps due to Mean Motion Resonance are clearly visible.

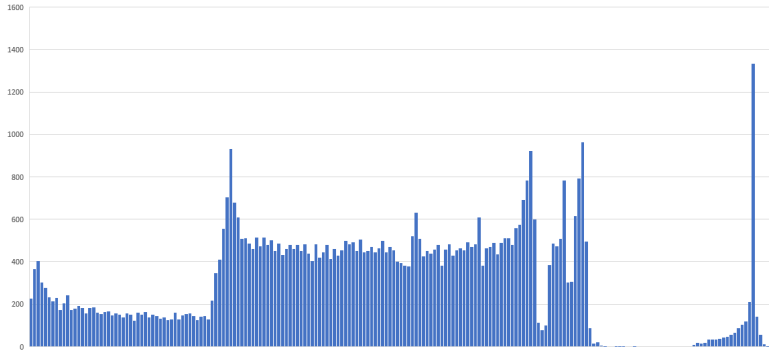


Figure 13.5 : Average Distance from sun for Asteroids over 10,000 years
The X-axis ranges from 0 to $1e12$ metres from the Sun.

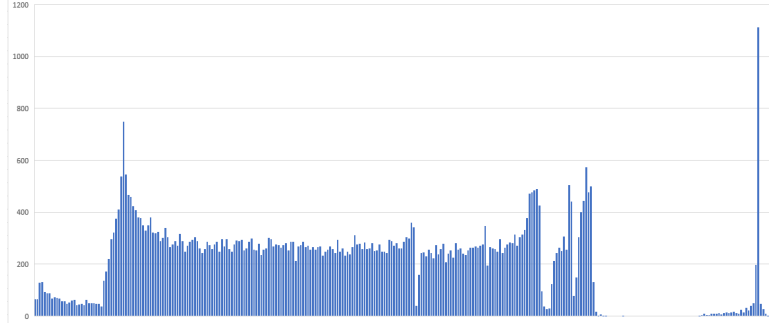


Figure 13.6 : Average Distance from sun for Asteroids over 15,000 years
The X-axis ranges from 0 to $1e12$ metres from the Sun.

12 Discussion on why Gaps are not Visible in the Main Belt Simulations

The reason that gaps in the distribution of semi major axes of the asteroids in the main asteroid belt is observed is due to Mean-Motion Resonance with the other planets, satellites etc. The resonance is best described by the fact that if an asteroid has a time period n and a larger mass orbitting around the sun has a time period m . If n and m are relatively

small numbers like 1,2,3,..7, there are certain time intervals during which the two bodies line up and the larger mass pulls the asteroid away from its orbit slightly. This happens to all asteroids and thus "gaps" are formed in the main belt.

The primary reason these gaps are not visible during direct simulation is due to the eccentricity of the asteroid orbits themselves. Owing to the relatively uniform distribution over a certain range, the orbits often overlap and their tracks are covered by transitioning asteroids, covering up the gap[3].

However if we inspect the cases where simulation is done over relatively short time spans say 1,000 - 10,000 years, there are visible gaps as the orbits are not completely erratic in their eccentricities yet. Especially referring to Figure 10.2, the effect is extremely visible in the distribution of asteroids against distance from the sun with one clear minima and smaller relatively less obvious mean motion resonance induced gaps in the distribution.

13 Scope for More Precise Results and Further Applications

The results obtained can be refined with a few changes listed below :

- Considering the eccentricity of Jupiter Orbit into calculation
- More refined methods of integration can be used over larger spans like the Wisdom-Holman Algorithm
- To view the exact distribution of semi-major axes of fewer number of simulated asteroids over a larger span of time in millions of years
- Perturbation with more than one planet, including Saturn and Mars, which give more realistic results

The calculations of the restricted three body problem can be extended to map trajectories of close-passing asteroids to other planets, if distant systems are considered, there also arises the question of whether once out of orbit an asteroid can be caught by a different stellar or planetary system. The most direct application of these calculations would be to simulate the rings of Saturn perturbed by its moons and treat it similarly as we have treated the asteroid belt.

14 Conclusion

The project initially started by testing out various integrators for numerically solving the differential equations related to basic orbital mechanics. After looking at the plots for deviations in energy, it was finally decided that the Euler-Richardson method worked best for this project. In parallel, knowledge about the governing equations for the reduced three body problem was also gathered from various sources.

Trajectories of the asteroids at various initial parameters was tested out which gave different results for different initial placements.

Finally, around 100,000 asteroids with varied initial parameters were generated and iterations were applied to each asteroid's parameters giving a final set of parameters after a considerable amount of time (thousands of years) which could be plotted. These plots resembled the Kirkwood gaps to a good accuracy given our approximations at the start.

15 Repository for Code Used for Simulation

<https://github.com/SahilSaha/Asteroid-Simulation>

References

- [1] Richard Frnka. *The Circular Restricted Three-Body Problem*, 2010.
https://jan.ucc.nau.edu/~ns46/student/2010/Frnka_2010.pdf
- [2] Ian R. Gatland , ”Numerical integration of Newton’s equations including velocity- dependent forces”, American Journal of Physics 62, 259-265 (1994).
<https://doi.org/10.1119/1.17610>
- [3] Maryam Tabeshian and Paul A. Wiegert. 2016 ApJ 818 159.
<https://doi.org/10.3847/0004-637X/818/2/159>